Management of a Solar-PV System with Energy Storage

Shital Thorat† and **Vaiju N. Kalkhambkar**, Non-members

ABSTRACT

A solar-PV system is generally connected to distributed generation (DG) by the utility grid. The solar inverter retains some capacity after active power generation. Reactive power compensation can be achieved by utilizing the remaining capacity of the solar-PV inverter. This paper introduces an energy management system (EMS) for real and reactive power management. The proposed EMS includes two modes: PV-STATCOM and islanding. In PV-STATCOM mode, the PI control is used whereas for the islanding mode, voltage frequency control is employed. This paper proposes the energy management of reactive power by utilizing the solar photovoltaic (PV) inverter as a static synchronous compensator (PV-STATCOM). Therefore, no other additional flexible AC transmission system controllers or series/shunt capacitors are required. During the islanding mode, the storage provides continuous supply to the load. The system is simulated using single-phase and three-phase modes with the hardware results also revealed. The proposed scheme provides a significant improvement in power factor while reducing the total harmonic distortion.

Keywords: PV-STATCOM, Reactive Power Control, Voltage Frequency Control Strategy, Islanding Mode

1. INTRODUCTION

The power system is interconnected and complex. The electrical power sector is experiencing continuous growth putting the distribution system under stress and affecting transmission capacity. The global energy crisis and the threat of environmental disruption have become common problems worldwide, exacerbated by the constantly increasing electricity demand. Carbon emissions from conventional power plants pose a serious threat to the environment. Other energy sources such as nuclear power plants can seriously endanger human safety. To overcome these concerns, researchers are paying close attention to renewable energy sources.

One of the most innovative research areas of power electronics technology is the integration of battery energy storage systems with renewable energy sources. Increasing grid integration with renewable energy sources requires control strategies to achieve reliability and stability [1]. Green energy sources such as solar farms contribute to the reduction in greenhouse gas emissions. Although PV farms are costly, they receive strong support from various global incentive programs [2, 3].

Recently, widespread research has been carried out in the renewable energy field. A solar farm consisting of a PV array, charge controllers, and inverters with controllers can obtain the highest possible energy level from solar power under all environmental conditions, but the operation must be optimized. To accomplish this, several approaches have been proposed such as maximum power point tracking (MPPT) [4]. The PV solar farm has gained popularity for its large and small-scale grid integration ability. A conventional solar-PV system is installed at the load side to reduce the distribution and transmission cost [2]. To reduce the loading stress on the transformers and grid, the load profile needs to be improved to reduce electrical loss in the feeder. Reactive power is the main system issue since it is required to maintain the voltage profile throughout the transmission lines. If reactive power is lacking in the transmission line, it needs to be supplied from reactive power sources such as STATCOM and FACTS devices. Reactive power compensation is required in the event of voltage sag and swell to maintain the voltage at 1 pu. Therefore, it is necessary to compensate reactive power to distribute sufficient power through the transmission line.

Transmission systems face challenges in the integration of renewable sources since they have limited power transfer capacity [5–10]. To enhance the available power transfer capacity of transmission lines, flexible AC transmission (FACTS) devices are employed. In some conditions, new transmission lines must be constructed which is a costly solution. Nowadays current source inverters (CSI) are preferred in PV applications since they provide active power to the load and work closely with the unity power factor

Manuscript received on October 24, 2019 ; revised on April 24, 2021 ; accepted on April 28, 2021. This paper was recommended by Associate Editor Kriangkrai Sooksood.

The authors are with the Department of Electrical Engineering, Rajarambapu Institute of Technology, Rajaramnagar, India.

†Corresponding author: shitalthorat64640@gmail.com

Digital Object Identifier 10.37936/ecti-eec.2021193.222654

[11]. Hence, separate capacitor banks need to be used to supply the required reactive power. The output of the PV panel depends upon irradiance and thus becomes zero during the nighttime or bad weather conditions. During zero output conditions, the PV inverter does not work. In this instance, the grid should supply the required power according to load demand. Hence, to take advantage of its full capacity at nighttime, the inverter is used to supply reactive power to the grid [9, 10, 12–15].

An inverter topology is proposed to interconnect the grid with the PV panel. Active power is produced during the daytime period, while reactive power is produced during weak insolation conditions, supplied by the inverter. Based on the requirement at the point of common coupling, reactive power is provided by the inverter [16–18]. As the main factor responsible for loss, reactive power is essential for maintaining the voltage profile throughout the transmission lines. In the absence of reactive power, auxiliary sources are required such as STATCOM and other FACTS devices. Voltage instability is a big challenge in power systems. In recent research, numerous power stability problems are linked with voltage instability. Reactive power compensation is used to increase voltage stability under critical operating conditions. Huge PV farms are capable of injecting reactive power into the grid.

Large electricity producers tend to be located away from existing power lines, thereby requiring more space. Thus, the PV systems are beneficial since they can be located anywhere to generate power. Islanding requires the continuous operation of solar power generation. Any malfunction in the grid is not detected by the solar power generation system and disconnection occurs immediately, leading to severe problems. Therefore, an adaptive control scheme must be used in protective devices to detect and address islanding issues. Renewable energy sources work in parallel with the power distribution network and utility grid malfunction can increase the chance of damage. Therefore, protective equipment should be used to actively detect and eliminate islanding issues. In normal operating conditions, the active and reactive power required by loads is supplied by the PV power generator and grid. New PV solar controllers such as STATCOM now offer many advantages over the conventional PV solar system such as increased power handling capability of the grid, overall system power improvement, voltage regulation, and low cost.

The point of common coupling (PCC) is balanced under normal conditions. Under islanding conditions, when the grid is disconnected, the PCC becomes unbalanced and hence the PV generation system can be connected. The PCC remains balanced when the output power of the PV generation system is equal to the load demand. When the frequency and voltage of the PV generation system are the same as the normal functioning grid, protective relays are prevented from functioning properly. Common islanding detection methods can be classified into passive and active detection methods. The passive islanding detection method monitors frequencies, phases, and voltages at the load end, leading to the detection of islanding conditions. The disturbances in system frequency and voltage are not equal to the limit set for relay detection when the power output of the PV generation system and total consumption difference is limited. Thus, the drawback of this method is the presence of a non-detection zone. In this paper, the passive voltage frequency (VF) method is used for islanding operations.

Islanding can lead to voltage unbalance as well as voltage and frequency instability in the power system, increasing the chance of damage. Islanding creates many problems in the power system such as interference, power quality, safety, voltage unbalance, as well as and voltage and frequency instability. Under emergency conditions, loads require a continuous power supply but this is cuts off due to islanding issues, and proper control is required to avoid such problems. The islanding control strategies control the voltage and frequency of the system and attempt to provide continuous supply to the load. Batteries are used for solar energy storage and power discharge if required. Each battery has different temperature, mounting, and ventilation requirements. Lead-acid batteries are preferred in solar energy because they give better results in terms of charging and discharging cycles. The batteries can be classified as flat plate or tubular, the latter being taller. The batteries are manufactured using three main chemical compositions: lead-acid, lithium-ion, and saltwater. The home solar system generates DC electricity which is converted into AC electricity using a charge controller and solar inverter. The battery stores this AC electricity for use at night or in the absence of sunlight.

This paper is based on energy management and contributes to the existing research on active and reactive power management and islanding mode control. The proposed energy management system provides reactive power support during the nighttime when the solar system is idle. Consequently, FACTS devices are not required, thereby making the system more cost-effective. Moreover, during the islanding mode of operation, the system provides continuous supply to the load, contributing to effective management of the system in the power sector.

This paper is arranged as follows: Section 2 provides the system model, while Section 3 describes the control system. Section 4 provides the results and discussion, while Section 5 presents the conclusion.

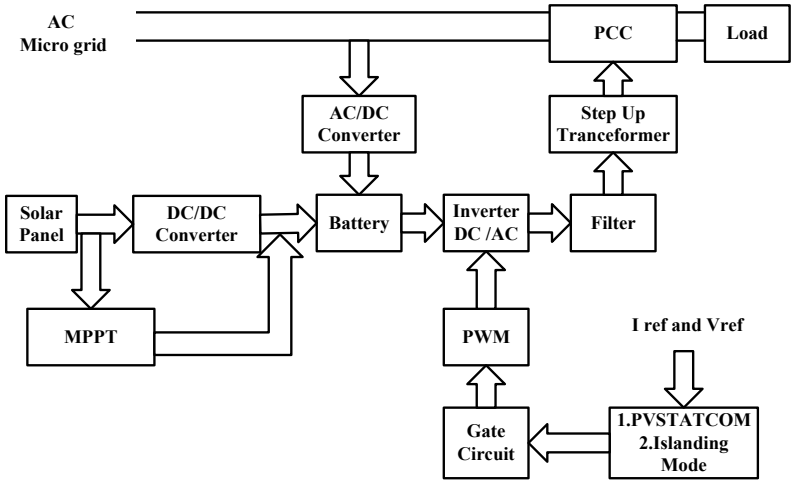

Fig. 1: *Block diagram of the proposed system model.*

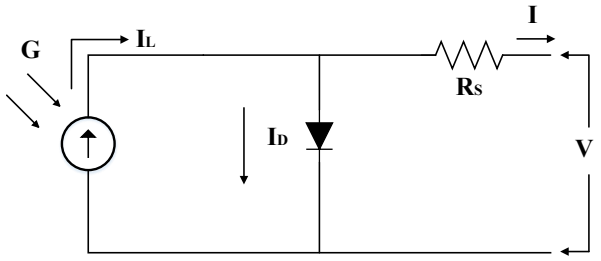

Fig. 2: *Equivalent electrical circuit of the PV cell.*

2. SYSTEM MODEL

Fig. 1 presents a block diagram of the proposed system model. The solar panel is connected to the battery through the MPPT and DC-DC converter. The MPPT provides a constant duty cycle for the DC-DC converter which in turn provides constant output to the battery. The battery provides a DC supply to the inverter. The transformer step-ups the voltage level from 12 V to 230 V. The proposed system works on two modes: PV-STATCOM and islanding. The AC to DC converter is used to charge the battery in the absence of solar supply.

2.1 Solar System

A solar cell is a basic component of the photovoltaic module. The power generated by the module is not sufficient to meet the required power demand. Several PV modules can be arranged in either parallel or series to increase the current (I) and voltage (V). Fig. 2 shows the equivalent electrical circuit model of the photovoltaic cell.

The characteristics of the PV cell are described by the following equations

$$I = I_L - I_D \tag{1}$$

The diode current can be expressed as

$$I_D = I_0 \left[\exp\left(\frac{q(V + IR_S)}{\gamma k T_C}\right)\right] \tag{2}$$

Put Eq. (2) into Eq. (1)

$$I = I_L - I_0 \left[\exp\left(\frac{q(V + IR_S)}{\gamma k T_C}\right)\right] \tag{3}$$

where $\gamma = A \cdot N_{CS} \cdot N_S$

$$I_L = \left[\left(\frac{G}{G_R}\right)\left(I_{LR} + \mu_{SC}\left(T_C - T_{CR}\right)\right)\right] \tag{4}$$

$$I_0 = I_{0R}\left(\frac{T_C}{T_{CR}}\right)^3 \exp\left[\left(\frac{q\varepsilon_0}{kA}\right)\left(\frac{1}{T_{CR}} - \frac{1}{T_C}\right)\right] \tag{5}$$

where I_L = light current, I_D = diode current, R_S = series resistance, k = Boltzmann constant, G = actual irradianc, q = electron charge, A= completion factor, ε_0 = material band gap energy, G_R = irradiance at reference condition, μ_{SC} = manufacturer-supplied temperature coefficient of short circuit current, I_0 = saturated current, I_{0R} = reverse saturated current, I_{LR} = light current under standard temperature coefficient of short circuit condition, T_C = actual cell temperature, γ = shape factor, T_{CR} = cell temperature at reference condition, N_S = number of series-connected modules, and N_{CS} = number of series-connected cells per module.

2.2 Inverter

The solar farm is modeled as a voltage source inverter and the output of the PV panel is DC. Thus, the DC source represents the PV panel. The total injection of active power depends on inverter input, i.e., the magnitude of the DC voltage. The zero active power injection operates when the DC source is disconnected, i.e., at nighttime.

The voltage source inverter involves the assembly of MOSFET switches and snubber circuits. A

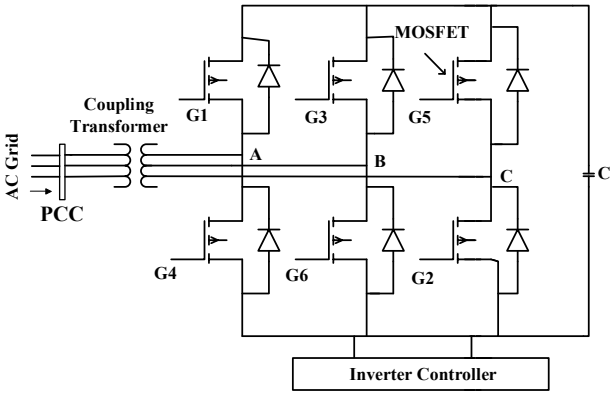

Fig. 3: *MOSFET based inverter using the STATCOM configuration.*

capacitor is employed to compensate for the ripples on the DC side. Each limb has two MOSFETs, converting the DC voltage into a series of pulsations with variable signal width according to the switching signals. The switching signal is based on the difference in the variable amplitude magnitudes of sinusoidal signals known as 'modulating signals' while the fixed-magnitude, high-frequency triangular signal is known as the 'carrier signal'. The controller operates the phase angle of the sinusoidal modulating signals and variable magnitude.

The modulating signals used for all three phases are equally spaced with a shift of 120°. Similar carrier waves are applied to all three limbs, known as the sinusoidal pulse width modulation technique [18]. In order to eliminate the harmonics, some filter equipment is needed on the AC side. In this strategy, the amplitude of the carrier signal is regulated to unity, thus the magnitude of the modulating signal is known as the modulation index (MI) [13]. In the pulse width modulation switching method, the magnitude of the voltage at the inverter output modulation phase and voltage angles are directly proportional to MI [13]. To control the modulation phase angle and index, two separate proportional integrator control loops are integrated with the voltage source inverter [18].

3. CONTROL SYSTEM

3.1 Control Topology for PV-STATCOM

Conventional controllers are only employed to regulate reactive power inverter output, along with the DC-link voltage control while maintaining the unity power factor [19]. The PCC values represent the input of the controller, converting voltage and current from ABC to $dq0$. In the conventional controller, PI controllers are utilized to regulate the values of MPPT and $dq0$. In the PWM switching method, the magnitude of the voltage angle and the voltage at the inverter output are directly proportional to the modulation phase angle and index [13]. The $dq0$ values are provided to generate the appropriate switching pulses using PWM to trigger the MOSFET switches, i.e., G1, G2, G3, G4, G5, and G6 of the inverter, as shown in Fig. 3. After tuning the values, they are converted back from $dq0$ to ABC values. The PWM converts the modulating signal components into a sinusoidal modulating signal which is then compared to the higher frequency fixed-magnitude carrier signal or triangular wave.

Exchanging the reactive power between the grid and PV-STATCOM is important for voltage control. To generate the current reference signal, the output of the voltage controller is given to the PI controller as shown in Fig. 4.

Fig. 4 shows a block diagram of the proposed control strategy. The feedback signals are sensed from PCC voltages and load current. The load current ABC frame is converted to $dq0$ frame. The PLL is used to synchronize the signals with the PCC voltage. Input currents of the three-phase loads are i_{abc}, which are transformed into the q axis component i_q and d axis component i_d with the dq transform, including DC and AC components. The low pass filter (LPF) with a cut-off frequency of 25 kHz is used to obtain the DC components (i_d and i_q) by passing the $dq0$ current component through it. The DC components i_q and i_d are obtained. The error between the sensed DC bus voltage (V_{dc}) and reference DC bus voltage (V_{dc}^*) is the input of the proportional integral (PI) controller. The output of the PI controller is i_{loss}, i.e., the loss component of the current, while V_{dc} is the difference between sensed DC voltage and reference at the n^{th} sampling instant. K_{id} and K_{pd} are the integral and proportional gains of the PI controller. The amplitude of the PCC voltage and reference values are given to the second PI controller to regulate the voltage. To regulate the AC voltage, the output value of the PI controller is added to the DC component of the i_q quadrature component of the current. Inverse Park's transformation is used to convert the $dq0$ current into reference source currents. Reference currents (i_{sa}^*, i_{sb}^*, i_{sc}^*) are used to generate gate pulses for the voltage source inverter[20–25].

3.2 Control Topology for the Islanding Mode

The regulation of distributed generators (DGs) in islanding is performed under the voltage frequency control. During islanding, at least one voltage source inverter must be operated in voltage frequency (VF) control mode to regulate the frequency and voltage of the system within permissible limits [26, 27].

The main advantage of this control topology is that no extra communication devices are required. Therefore, only local measurements and the plug-and-play operation are included. The voltage source inverter adopted for voltage frequency control in the block

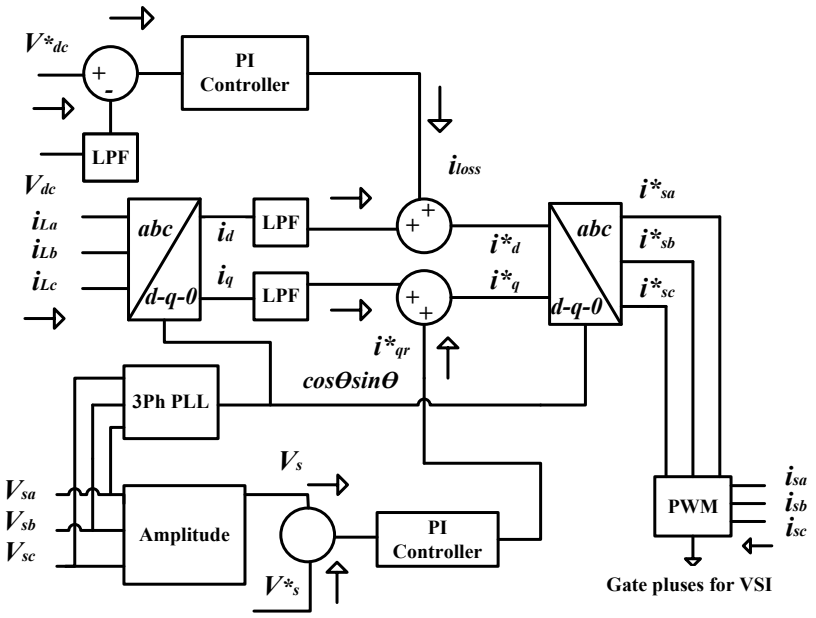

Fig. 4: *Block diagram of the proposed control strategy.*

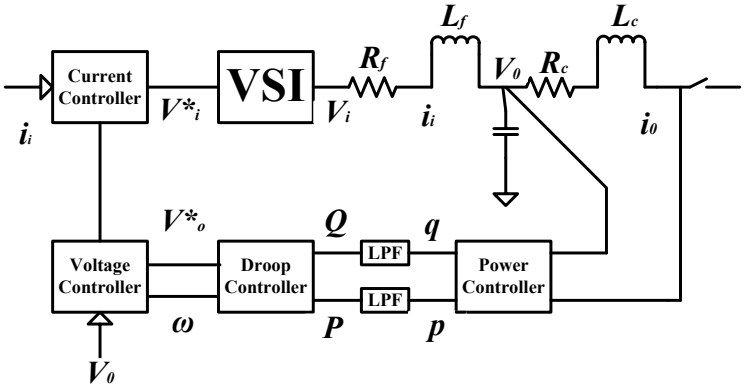

Fig. 5: *General block diagram of the VF control topology.*

diagram is shown in Fig. 5.

This control strategy includes three controllers: current, voltage, and droop. According to real and reactive power sharing and droop characteristics, the droop controller determines the frequency and magnitude of the inverter output voltage. To offset the disturbances of high frequency and add value to the output voltage of voltage source converter (VSC), current and voltage controllers are designed. Instantaneous reactive and real power components in the *d-q* frame are defined by measuring the output current and voltage.

The reactive and active power injected into the AC system by a renewable energy source are calculated according to Eqs. (6) and (7).

$$P = \frac{3}{2}[V_d * i_d + V_q i_q] \tag{6}$$

$$Q = \frac{3}{2}[-V_d * i_q + V_q i_d] \tag{7}$$

where V_d and V_q are the voltage components of the *dq* frame of the AC system and cannot be controlled by the VSC system. i_d and i_q are the current components of the *dq* frame of the AC system. When the phase lock loop (PLL) is in steady state, $V_q = 0$ and Eqs. (6) and (7) can be written as

$$P = \frac{3}{2}V_d * i_d \tag{8}$$

$$Q = -\frac{3}{2}V_d * i_q \tag{9}$$

The reactive and active power share between voltage and frequency based on drop gain can be written as

$$v^* = v_n - n_q Q \tag{10}$$

$$\omega \ = \omega_n - m_p P \tag{11}$$

where v^* and ω show the reference output voltage and frequency of inverters, while ω_n and v_n are their

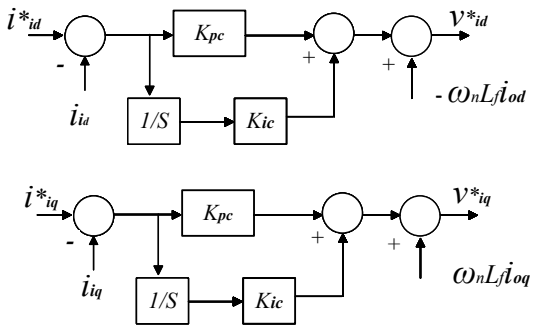

Fig. 6: *Block diagram of the voltage controller.*

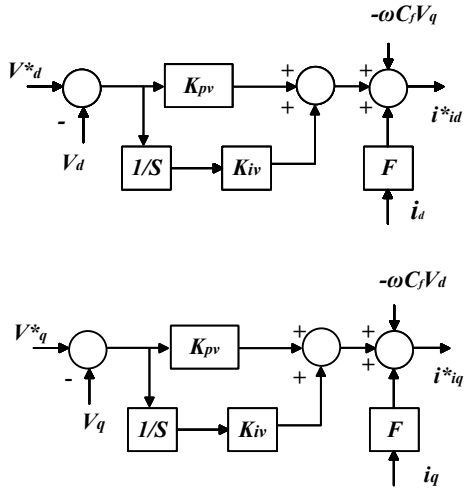

Fig. 7: *Block diagram of the current controller.*

nominal values, respectively. m_p and n_q are the droop gains of P-ω and Q-v, respectively.

$$m_p = \frac{\omega_{\max} - \omega_{\min}}{P_{\max}} \tag{12}$$

$$n_q = \frac{V_{d\max} - V_{d\min}}{Q_{\max}} \tag{13}$$

where $\omega_{\min}$ and $\omega_{\max}$ are the minimum and maximum frequency magnitudes. $V_{d\min}$ and $V_{q\max}$ are the minimum and maximum voltage magnitudes of the dq frame.

Droop control topology is based on locally measured data and does not depend on communication signals, thereby eliminating the difficulties imposed by physical location. The droop method has other advantages such as flexibility, high reliability, structure simplicity, easy implementation, free laying, and different power ratings. In power grids, reactive and active power exhibit strong coupling with frequency and the voltage, respectively. The drop controller output is delivered to the voltage controller. The output of the droop controller is given to the voltage controller, as is shown in Fig. 6.

Voltage controller equations can be written as

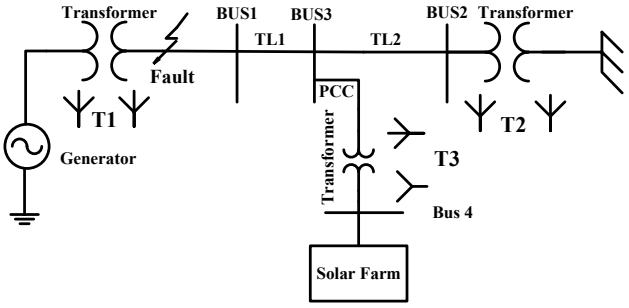

Fig. 8: *Single line diagram of the system.*

$$v_{id}^* = \left(K_{pc} + \frac{K_{ic}}{S}\right)(i_{id}^* - i_{id}) - \omega_n L_f i_{od} \tag{14}$$

$$v_{iq}^* = \left(K_{pc} + \frac{K_{ic}}{S}\right)(i_{iq}^* - i_{iq}) + \omega_n L_f i_{oq} \tag{15}$$

where v_{id}^* and v_{iq}^* are the AC system dq frame common reference voltage components. K_{pc} is a proportional gain and K_{ic} is an integral gain. Axis dq is set as a common reference frame rotating at frequency ω_n. L_f is the inductance of the LC filter.

Fig. 7 presents a block diagram of the current controller. Axis $dq$is set as a common reference frame rotating at frequency ω_n while i_{id}^* is the current of the reference frame of i^{th} inverters and at d axis and i_{iq}^* is the current of the reference frame of i^{th} inverters at q axis. i_{id} and i_{iq} are currents of the dq frame. i_{oq} is the output current of the inverter of the q frame.

The current control loop is considered as a conventional PI controller as shown in Fig. 7. The output of the current controller is given to the inverter for switching.

$$i_{id}^* = \left(K_{pv} + \frac{K_{iv}}{S}\right)(V_{od}^* - V_{od}) + F i_{od} - \omega_n C_f V_{oq} \tag{16}$$

$$i_{iq}^* = \left(K_{pv} + \frac{K_{iv}}{S}\right)(V_{oq}^* - V_{oq}) + F i_{oq} + \omega_n C_f V_{od} \tag{17}$$

where K_{pv} is proportional gain and K_{iv} is integral gain. v_{od} and v_{oq} are output voltages of the inverter in the dq frame. v_{od}^* and v_{oq}^* are output reference voltage variables of the inverter on the dq frame. i_{oq} is output current of the inverter in the q frame. F is frequency. C_f is the capacitor of the LC filter.

4. RESULTS AND DISCUSSION

4.1 Case Study

Fig. 8 presents a single line diagram of the system. The system under study usually contains a single, large capacity synchronous generator with a voltage of approximately 22 kV at 50 Hz frequency, stepping up to 400 kV using a transformer. It has a large

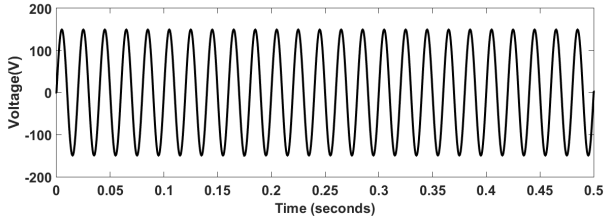

Fig. 9: *Input grid voltage.*

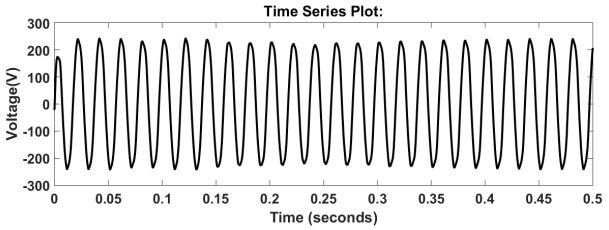

Fig. 10: *Voltage across load.*

transmission line. The T1 is a step-up transformer while T2 is a step-down transformer. The PV farm has a large capacity and is connected through a coupling transformer to the transmission line at the midpoint, i.e., at the PCC. The 100 W model is considered in the proposed system to simulate the implementation of the modeling and hardware. The proposed system consists of a solar panel, MPPT, boost converter, battery, inverter, and microgrid. The PV system has 12 V rating, 5 A, and 60 W, connected to batteries (12 V 7 Ah and 24 V 7 Ah) through a boost converter and MPPT. The battery is connected to the voltage source inverter which injects the power into the microgrid through the PCC. The proposed 100 W system is modeled in the MATLAB Simulink environment. The MATLAB simulation is performed in two parts: single and three-phase.

4.2 Single-phase System

The single-phase 100W system is simulated in two modes: PV-STATCOM and islanding.

4.2.1 PV-STATCOM mode

In faulty conditions, the voltage of the supply system is less than that of the standard grid. The PV inverter injects the reactive power into the grid voltage through the PCC. The 46 W load is connected to the supply system. The supply voltage is less than the standard voltage, thereby meeting the load demand. Fig. 9 shows the input voltage of the PV-STATCOM mode.

Fig. 9 shows the supply voltage during faulty conditions as 150 V. The load requires 46 W power but the supply system is unable to fulfill this demand. Therefore, the PV inverter supplies reactive power to fulfill the load demand. After the injection of reactive

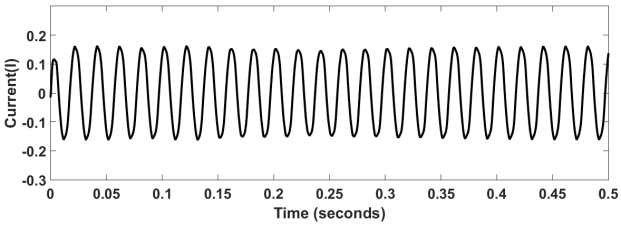

Fig. 11: *Load terminal current.*

power, the supply voltage is increased to that of the standard grid. If the fault occurs in the microgrid during the day, the grid load supply is halted and load demand is immediately fulfilled by the PV system.

Fig. 10 shows the increase in voltage after an injection of power. Voltage oscillations are damped out using a damping oscillator.

Fig. 11 shows the current waveform after voltage recovery and fault clearing.

4.2.2 Islanding mode

Fig. 12 shows the current waveform at the grid supply terminal in the islanding mode of operation. From 0–1 s, the supply from grid to load is in the ON state and from 1–2 s there is no supply from the grid (i.e., grid failure). During this 1–2 s period, power is supplied through solar generation, and present in the grid from 0–1 s.

Fig. 13 shows the current waveform of the solar generation. The solar system injects the power from 1–2 s when the grid is in the OFF state.

Fig. 14 shows the voltage waveforms of the islanding mode of operation across the load. From 0–1 s, the voltage waveform is off-grid whereas from 1–2 s, the voltage waveform is received by solar power injection. It is clear from Fig. 14 that grid and solar power generation voltages are approximately the same, and thus the supply to the load is maintained continuously. Fig. 15 shows the voltage waveform of the solar power injection and the sinusoidal voltage supplied to the load.

The PV and grid are used to charge the battery. In cloudy conditions, the PV solar panel is unable to provide sufficient voltage to the battery. The battery discharging level is set at 30% to avoid damage and improve its life. A charging level of below 25% directly affects the life of the battery. It is possible to combine the islanding and battery charging modes. To charge the battery, the grid voltage is reduced to 12 V by the step-down transformer while the AC voltage is converted into DC using a rectifier. The output voltage of the rectifier is given to the battery terminals for charging. The initial charge of the battery is set at 30% at which point the charging begins. The state of charge (SOC) for battery is shown in Fig. 16.

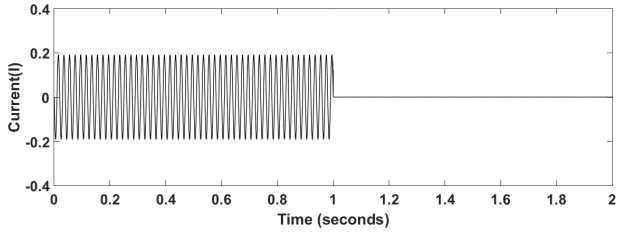

Fig. 12: *Grid supply terminal current.*

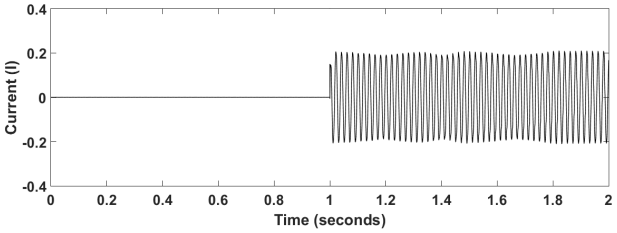

Fig. 13: *Solar generation current.*

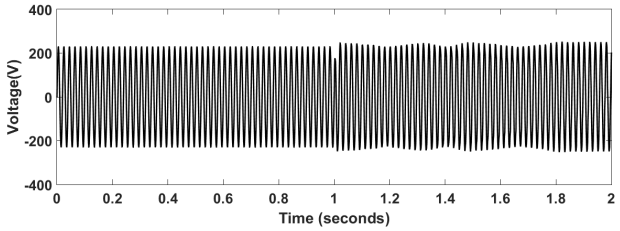

Fig. 14: *Voltage across the load.*

4.3 Hardware Results

The proposed hardware prototype hardware is shown in Fig. 17. It consists of a single-phase supply system, connected to the grid and load. The inverter has a separate driver circuit, designed with an IC 4047. The prototype hardware has a 60 W solar panel and three lead-acid batteries. In PV-STATCOM mode, one 12 V 7 Ah battery is used, while for islanding mode of operation, two 12 V 7 Ah batteries are connected in series to provide a 24 V supply to the inverter. Batteries supplying 12 V and 24 V are provided to the driver circuit of the inverter.

Fig. 18 shows the voltage at the point of common coupling when PV-STATCOM is connected to the grid. The grid supply is provided to the load through the PCC, while voltage sag is created in the system through the transformer. The load and transformer are interconnected through the PCC. When the grid supply to the load is on, it flows into the transformer. Voltage drop occurs in the transformer due to winding (inductor coil). The voltage is increased to 243 V with the help of PV-STATCOM to mitigate sag. The output waveform is almost sinusoidal with a total harmonic distortion of 2%.

Fig. 19 shows the current at the point of common coupling (PCC) when PV-STATCOM is connected to the grid. After voltage sag, the current is restored to 0.39 A.

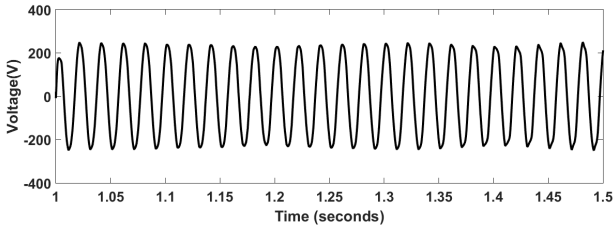

Fig. 15: *Voltage after solar power injection to the load.*

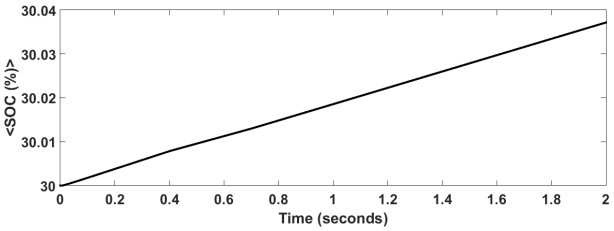

Fig. 16: *State of charge for the battery.*

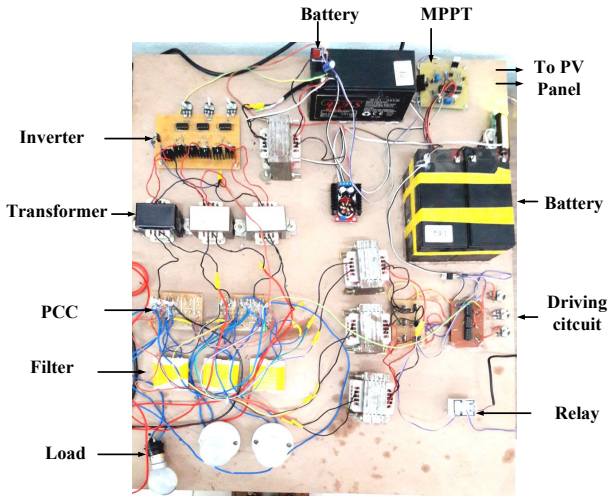

Fig. 17: *Prototype of the hardware model.*

Fig. 20 shows the active and reactive power at the PCC when the 10 W load is connected. In a faulty environment, the active power without PV-STATCOM at the PCC is 14.4 W while apparent power is 19.4 VA. The power factor is 0.945 which is low for industrial application.

Fig. 21 shows the output power value of the proposed system using PV-STATCOM. From the foregoing, it is clear that grid power transfer is increased from 19.4 VA to 31 VA with the use of PV-STATCOM. Reactive power is supplied by PV-STATCOM to maintain the level of 230 V. According to these power values, it is clear the proposed system results in increased grid power.

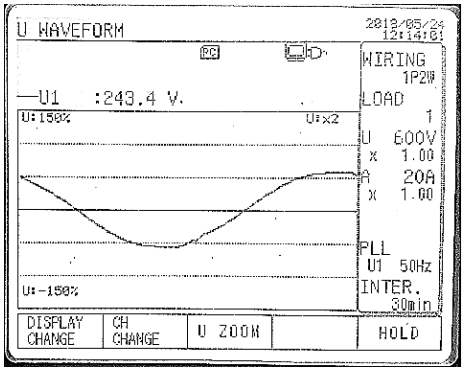

Fig. 18: *Voltage at the PCC with PV-STATCOM.*

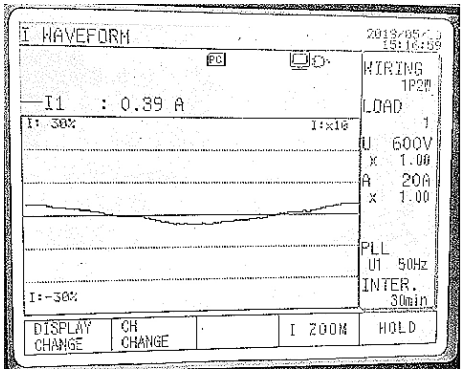

Fig. 19: *Current at the PCC with PV-STATCOM.*

Table 1: *Camparison of grid power without STATCOM and with STATCOM.*

	Total Power (VA)	Reactive Power (VAR)	Power Factor
Grid Power without STATCOM	19.4	14.1	0.945
Grid Power with STATCOM	31	22	1

Table 2: *Camparison of THD analysis without STATCOM and with STATCOM.*

	Voltage (V)	THD (%)
Without STATCOM	160	12
With STATCOM	244	2

Table 1 compares the grid power without STATCOM and with STATCOM.

The THD analysis of the inverter output voltage performed during faulty conditions using power analyzer equipment is presented in Fig. 22. The THD of the voltage waveform is 12% which is more than the IEEE standard. According to the IEEE standard, THD should be less than 5%. The THD analysis of the inverter output voltage after fault clearance is

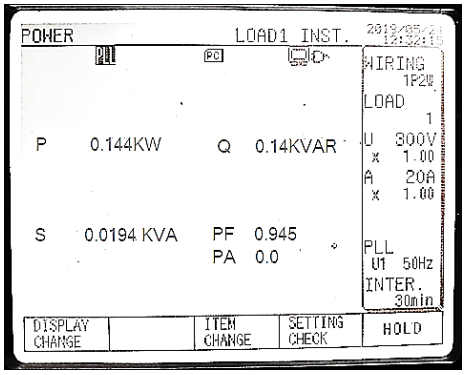

Fig. 20: *Grid power without PV-STATCOM.*

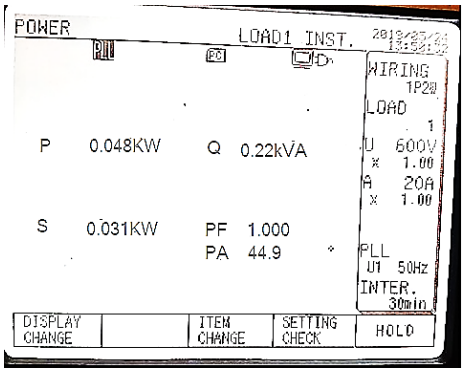

Fig. 21: *Grid power with PV-STATCOM.*

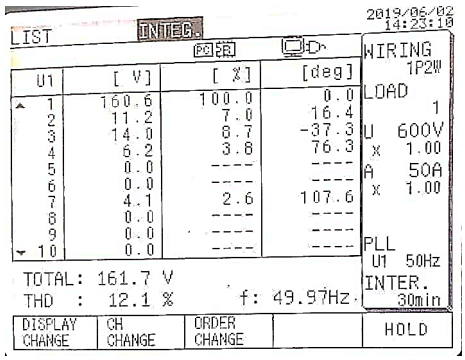

Fig. 22: *THD analysis without PV-STATCOM.*

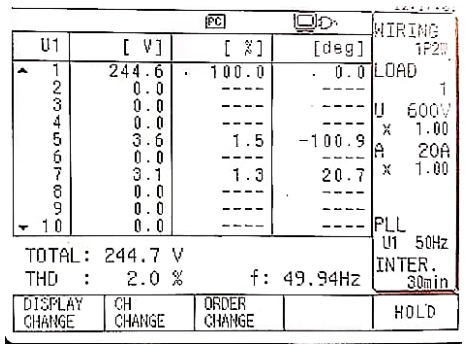

Fig. 23: *THD analysis with PV-STATCOM.*

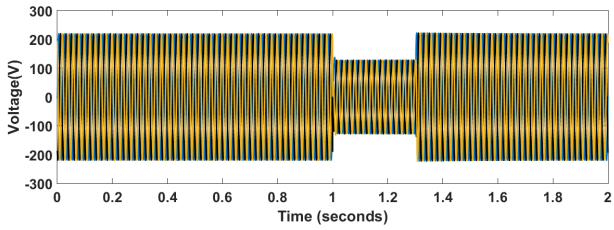

Fig. 24: *Voltage during faulty conditions.*

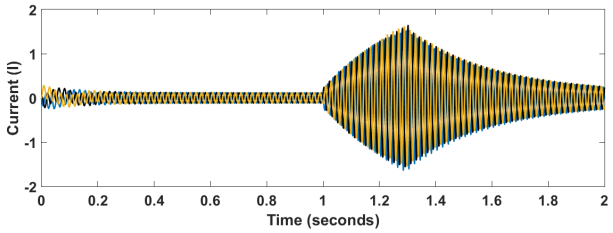

Fig. 25: *Current during faulty conditions.*

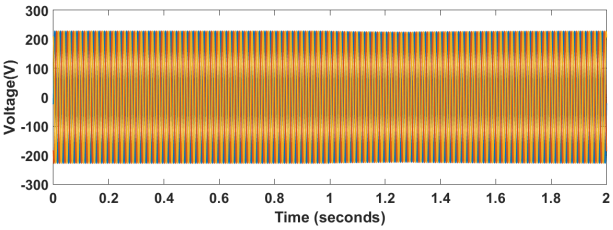

Fig. 26: *Voltage after the injection of reactive power.*

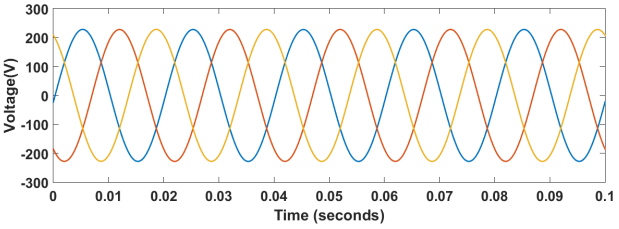

Fig. 27: *Voltage waveform following fault clearance.*

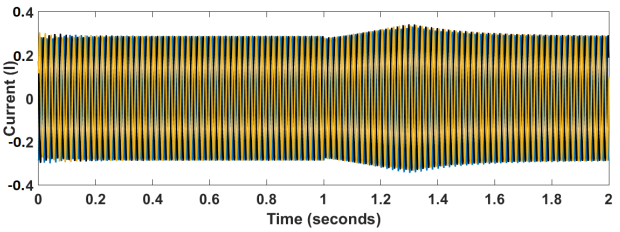

Fig. 28: *Current after the injection of reactive power.*

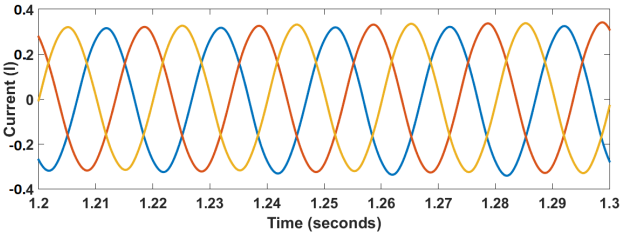

Fig. 29: *Current waveform after fault clearance.*

also presented in Fig. 22. The THD of the voltage waveform is 2%. The THD analysis is performed using power analyzer equipment indicates that THD is within the permissible limit according to the IEEE standard.

Table 2 compares the THD analysis without STATCOM and with STATCOM.

4.4 Three-Phase System

The three-phase 100 W system is simulated in two modes: PV-STATCOM and islanding.

4.4.1 PV-STATCOM mode

In the three-phase transmission line, the fault occurs during the 1–1.3 s period. In faulty conditions, the voltage drops in the transmission line and the current is much higher. When a fault occurs in the system, it draws more current and the voltage drops to $V = I \cdot R$. Therefore, a power loss occurs in the transmission line. In such a situation, the system needs reactive power.

Fig. 24 shows the voltage versus time characteristics. When a fault occurs on the transmission line (short circuit), the current increases suddenly and the voltage drops. These results also indicate power loss in the transmission line.

Fig. 25 shows the current waveform during faulty conditions. The current increases suddenly during the faulty conditions.

Following fault clearance, the current starts to decrease and attempts to stabilize. After a few seconds the current returns to normal.

After the injection of reactive power, the voltage of the line increases. Fig. 26 shows the voltage waveform after the injection of reactive power. The drop in voltage during faulty conditions is nullified.

Fig. 27 presents an enhanced view of the voltage waveform following fault clearance.

The current waveform returns to the normal limit after the injection of reactive power, as shown in Fig. 28. The reactive power of the line prior to the injection of reactive power is 144 VAR. Following the injection of reactive power injection by the PV inverter, the total reactive power is 220 VA.

Fig. 29 shows the current waveform after fault clearance.

4.4.2 Islanding mode

In this study, the islanding mode is simulated using two breakers, the first of which is connected after the three-phase source. Initially, this breaker is closed. From 1–2 s, the breaker is open and supply to the load is cut off during this time and islanding occurs.

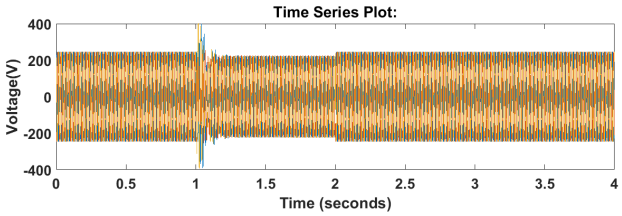

Fig. 30: *Voltage waveform of the islanding mode.*

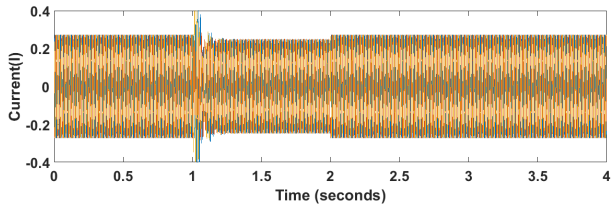

Fig. 31: *Current waveform of the islanding mode.*

After 2 s, the breaker closes again and the grid can provide supply to the load.

The second breaker is connected to the PV system after the injection transformer. This breaker is initially open. From 1–2 s, the breaker is closed and can provide supply to the load during islanding. After 2 s, the breaker reverts to the original open position and the grid is available to supply the load. The inverter is designed for a 700 W load. The output of the inverter is 13.45 V. The transformer is used to step up the voltage of the inverter to produce an output voltage of 230 V.

Fig. 30 shows the voltage waveform of the islanding mode. From 0–1 s, the grid is present, while from 1–2 s the grid supply is absent and the PV inverter provides the supply. During the switching of the breaker, some harmonies are produced. After 2 s, the grid is able to provide supply and the PV inverter supply is cut off. When islanding occurs, the PV system provides supply to the load, when the power source harmonics enter the system and the voltage spike comes into play for a small interval due to a sudden disconnection in the grid and the PV is connected.

Fig. 31 shows the current waveform during the islanding mode. During switching, some harmonics are created in the system.

Fig. 32 shows the SOC of the battery when a 0–1 s and 2–4 s microgrid supply is available to enable the battery and solar panel to charge through the grid.

In cloudy conditions, the PV solar panel is unable to provide sufficient voltage to the battery. During this period, the microgrid provides the supply to charge the battery. From 1–2 s, the grid supply is unviable (islanding mode), and the battery starts to discharge during this period due to the VSI providing supply to the load.

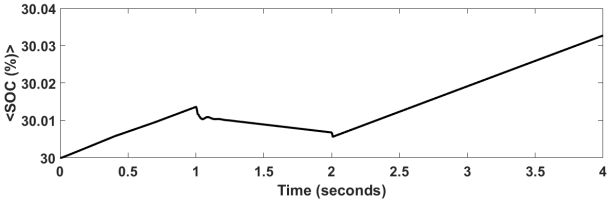

Fig. 32: *SOC for the battery.*

5. CONCLUSION

In this paper, PV-STATCOM and islanding mode topology is discussed. The PV solar farm is inoperative during the nighttime. The proposed topology utilizes the PV inverter as STATCOM during the nighttime, thereby improving the power transfer capacity with the full capacity of solar inverter. Furthermore, during the day, the inverters have remaining capacity after active power production, and this can be employed to increase the power transfer capability. The results show an improvement in the power transfer capability of the grid. Therefore, the proposed control technique helps to reduce the need for expensive FACTS devices and series/parallel capacitors. During the proposed islanding mode, the storage facility provides supply to the load, resulting in continuous power. The charging of the battery through the solar panel as well as the grid is done. Therefore, active and reactive power management is done by using proposed control strategies.

REFERENCES

[1] R. K. Varma, S. A. Rahman, and R. Seethapathy, "Novel control of grid connected photovoltaic (PV) solar farm for improving transient stability and transmission limits both during night and day," in *Proceedings of 21st World Energy Congress*, Montreal, Canada, 2010.

[2] R. G. Wandhare and V. Agarwal, "Reactive Power Capacity Enhancement of a PV-Grid System to Increase PV Penetration Level in Smart Grid Scenario," *IEEE Transactions on Smart Grid*, vol. 5, no. 4, pp. 1845–1854, July 2014.

[3] R. K. Varma, V. Khadkikar, and R. Seethapathy, "Night time application of PV solar farms STATCOM to regulate grid voltage," *IEEE Transactions on Energy Conversion*, vol. 24, no. 4, pp. 983–985, Dec. 2009.

[4] Y. Mahmoud and E. El-Saadany, "Accuracy improvement of the ideal PV model," *IEEE Transaction on Sustainable Energy*, vol. 6, no. 3, pp. 909–911, July 2015.

[5] H. Shen, H. Li, B. Huang, and J. Li, "Study on Integration and Transmission of Large Scale Wind Power in JiuQuan Area Gansu Province

China," in *CIGRE/IEEE PES Joint Symposium Integration of Wide-Scale Renewable Resources into the Power Delivery System*, Calgary, AB, Canada, 2009.

[6] Y. Xiao, Y. H. Song, C.-C. Liu, and Y. Z. Sun, "Available transfer capability enhancement using FACTS devices," *IEEE Transactions on Power Systems*, vol. 18, no. 1, pp. 305–312, Feb. 2003.

[7] X. P. Zhang, L. Yao, K. Godfrey, and C. Sasse, "Increasing the transfer of wind power on transmission network through coordinated FACTS control," *CIGRE Transactions*, C6-308, 2006.

[8] "FACTS solution to integrate wind power and enhance grid reliability," ABB, Aug. 2009 [Online]. `http://www.abb.com`

[9] X.P. Zhang, E. Handschin, and M. Yao, "Modeling of the Generalized Unified Power Flow Controller (GUPFC) in a Nonlinear Interior Point OPF," *IEEE Power Engineering Review*, vol. 21, no. 8, p. 57, Aug. 2001.

[10] A. D. Shakib, E. Spahic, and G. Balzer, "Optimal location of series FACTS devices to control line overloads in power systems with high wind feeding," in *2009 IEEE Bucharest PowerTech*, 2009.

[11] L. K. Haw, M. Dahidah, and N. Marium, "Cascade Multilevel Inverter based STATCOM with Power Factor Correction Feature," in *2011 IEEE Conference on Sustainable Utilization and Development in Engineering and Technology (STUDENT)*, Selangor, Malaysia, Oct. 2011, pp.12–18.

[12] R. K. Varma, S. A. Rahman, and T. Vanderheide, "New Control of PV Solar Farm as STATCOM (PV-STATCOM) for Increasing Grid Power Transmission Limits During Night and Day," *IEEE Transactions on Power Delivery*, vol. 30, no. 2, pp. 755–763, Apr. 2015.

[13] N. G. Hingorani and L. Gyugyi, *Understanding FACTS: Concepts and Technology of Flexible AC Transmission Systems*. Hoboken, NJ, USA: Wiley- IEEE Press, 1999.

[14] "ERCOT Competitive Renewable Energy Zones (CREZ) Transmission Optimization Study," ERCOT, Apr. 2, 2008 [Online]. `http://www.ercot.com`

[15] F. L. Albuquerque, A. J. Moraes, G. C. Guimarães, S. M. R. Sanhueza, and A. R. Vaz, "Photovoltaic solar system connected to the electric power grid operating as active power and reactive power compensator," *Solar Energy*, vol. 84, no. 7, pp. 1310–1317, 2010.

[16] R. M. Mathur and R. K. Varma, *Thyristor-Based FACTS Controllers for Electrical Transmission Systems*. Hoboken, NJ, USA: Wiley-IEEE Press, 2002.

[17] R. K. Varma, W. Litzenberger, A. Ostadi, and S. Auddy, "Bibliography of FACTS: 2005-2006 Part I IEEE Working Group Report," in *2007 IEEE Power Engineering Society General Meeting*, Tampa, FL, USA, Jun 2007.

[18] A. Beekmann, J. Marques, E. Quitmann and S. Wachtel, "Wind energy converters with FACTS Capabilities for optimized integration of wind power into transmission and distribution systems," in *2009 CIGRE/IEEE PES Joint Symposium Integration of Wide-Scale Renewable Resources Into the Power Delivery System*, Calgary, AB, Canada, 2009.

[19] K. R. Padiyar and R. K. Varma, "Damping torque analysis of static VAR system controllers," *IEEE Transactions on Power Systems*, vol. 6, no. 2, pp. 458–465, May 1991.

[20] M. H. Rashid, *Power Electronics Handbook: Devices, Circuits, and Applications*. London, UK: Academic Press, 2001.

[21] H. F. Wang, "Phillips–Heffron model of power systems installed with STATCOM and applications," *IEE Proceedings – Generation, Transmission and Distribution*, vol. 146, no. 5, pp. 521–527, Sept. 1999.

[22] CIGRE Task Force, "Impact of Interactions among Power System Controls", CIGRE Technical Brochure 166, Paris, France, 2000.

[23] S.-K. Kim, J.-H. Jeon, C.-H. Cho, E.-S. Kim, and J.-B. Ahn, "Modeling and simulation of a grid-connected PV generation system for electromagnetic transient analysis," *Solar Energy*, vol. 83, no. 5, pp. 664–678, May 2009.

[24] M. F. Schonardie and D. C. Martins, "Three-phase grid-connected photovoltaic system with active and reactive power control using dq0 transformation," in *2008 IEEE Power Electronics Specialists Conference - PESC 2008*, Rhodes, Greece, 2008.

[25] N. Pogaku, M. Prodanovic and T. C. Green, "Modeling, Analysis and Testing of Autonomous Operation of an Inverter-Based Microgrid," *IEEE Transactions on Power Electronics*, vol. 22, no. 2, pp. 613–625, Mar. 2007.

[26] F. Z. Peng, Y. W. Li and L. M. Tolbert, "Control and protection of power electronics interfaced distributed generation systems in a customer-driven microgrid," in *2009 IEEE Power & Energy Society General Meeting*, 2009.

[27] H. Kanchev, D. Lu, F. Colas, V. Lazarov and B. Francois, "Energy Management and Operational Planning of a Microgrid With a PV-Based Active Generator for Smart Grid Applications," *IEEE Transactions on Industrial Electronics*, vol. 58, no. 10, pp. 4583–4592, Oct. 2011.

Shital Thorat received her B.Eng. degree in Electrical Engineering from Shivaji University Maharashtra, India and M. Tech. degree in Electrical Power Systems from KES's Rajarambapu Institute of Technology affiliated to Shivaji University Maharashtra, India in 2019. She is currently a student member of IEEE. She is currently working as a Trainee Engineer in Bharat Petroleum Corporation Limited, Mumbai, India. She is also serving as a reviewer for various international journals. Her research activities involve renewable energy sources with energy storage system, power system, and smart grid. She has published 1 peer-reviewed journal and 2 conference papers.

Vaiju N. Kalkhambkar received his B.Eng. degree in Electrical Engineering in 1999 and Master's degree in Power Systems in 2004, both from Government College of Engineering, Karad, Maharashtra, India in 1999. In 2008 he got certified as Energy Manager from Bureau of Energy Efficiency (BEE) Government of India. He received his Ph.D. in Electrical Engineering from the Malaviya National Institute of Technology (MNIT), Jaipur, India in 2017. He is currently working as an Associate Professor and Head of Electrical Engineering Department at Rajarambapu Institute of Technology Rajaramnagar, Islampur, Sangli, Maharashtra, India. He is currently a senior member of IEEE, life member ISTE, IETE and IE (India). He has 16 years of experience in teaching in the electrical domain and 4 years of research experience. He has published more than 20 research papers in international and national journals and conferences. He has supervised about 25 B.Tech. and M. Tech. theses. He has handled various consultancy projects and energy auditing projects and received government funding for various funding schemes. He is also serving as a reviewer for various international journals of IEEE, Springer and Taylor & Francis. He has reviewed more than 60 international journals. His research interests include power systems, smart grid, renewable energy sources, power system optimization, and electric vehicles.